

Longitudinal optical monitoring of blood flow in breast tumors during neoadjuvant chemotherapy

This content has been downloaded from IOPscience. Please scroll down to see the full text.

2017 Phys. Med. Biol. 62 4637

(<http://iopscience.iop.org/0031-9155/62/12/4637>)

View [the table of contents for this issue](#), or go to the [journal homepage](#) for more

Download details:

IP Address: 128.91.43.237

This content was downloaded on 22/05/2017 at 21:27

Please note that [terms and conditions apply](#).

You may also be interested in:

[Clinical applications of near-infrared diffuse correlation spectroscopy and tomography for tissue blood flow monitoring and imaging](#)

Yu Shang, Ting Li and Guoqiang Yu

[Diffuse optics for tissue monitoring and tomography](#)

T Durduran, R Choe, W B Baker et al.

[Bulk optical properties of healthy female breast tissue](#)

T Durduran, R Choe, J P Culver et al.

[High-field small animal magnetic resonance oncology studies](#)

Louisa Bokacheva, Ellen Ackerstaff, H Carl LeKaye et al.

[Noninvasive characterization of the healthy human manubrium using diffuse optical spectroscopies](#)

Parisa Farzam, Claus Lindner, Udo M Weigel et al.

[Time-domain scanning optical mammography: II](#)

Dirk Grosenick, Heidrun Wabnitz, K Thomas Moesta et al.

[The effects of healthy aging on cerebral hemodynamic responses to posture change](#)

Brian L Edlow, Meeri N Kim, Turgut Durduran et al.



RayStation
HARMONIZE YOUR
TREATMENT PLANNING

INTRODUCING
RAYSTATION 6
WITH SUPPORT FOR
TOMOTHERAPY*

*Subject to regulatory clearance in some markets.

Longitudinal optical monitoring of blood flow in breast tumors during neoadjuvant chemotherapy

J M Cochran¹, S H Chung¹, A Leproux², W B Baker^{1,3},
D R Busch^{1,4}, A M DeMichele⁵, J Tchou⁶, B J Tromberg²
and A G Yodh¹

¹ Department of Physics and Astronomy, University of Pennsylvania, 209 S 33rd St, Philadelphia, PA 19104, United States of America

² Beckman Laser Institute, University of California Irvine, Irvine, CA 92612, United States of America

³ Department of Anesthesiology and Critical Care, Hospital of the University of Pennsylvania, Philadelphia, PA 19104, United States of America

⁴ Division of Neurology, Children's Hospital of Philadelphia, Philadelphia, PA 19104, United States of America

⁵ Department of Medicine (Hematology/Oncology), Hospital of the University of Pennsylvania, Philadelphia, PA 19104, United States of America

⁶ Department of Surgery, Hospital of the University of Pennsylvania, Philadelphia, PA 19104, United States of America

E-mail: cochranj@sas.upenn.edu

Received 10 February 2017, revised 24 March 2017

Accepted for publication 12 April 2017

Published 16 May 2017



CrossMark

Abstract

We measure tissue blood flow markers in breast tumors during neoadjuvant chemotherapy and investigate their correlation to pathologic complete response in a pilot longitudinal patient study ($n = 4$). Tumor blood flow is quantified optically by diffuse correlation spectroscopy (DCS), and tissue optical properties, blood oxygen saturation, and total hemoglobin concentration are derived from concurrent diffuse optical spectroscopic imaging (DOSI). The study represents the first longitudinal DCS measurement of neoadjuvant chemotherapy in humans over the entire course of treatment; it therefore offers a first correlation between DCS flow indices and pathologic complete response. The use of absolute optical properties measured by DOSI facilitates significant improvement of DCS blood flow calculation, which typically assumes optical properties based on literature values. Additionally, the combination of the DCS blood flow index and the tissue oxygen saturation from DOSI permits investigation of tissue oxygen metabolism. Pilot results from four patients suggest that lower blood flow in the lesion-bearing breast

is correlated with pathologic complete response. Both absolute lesion blood flow and lesion flow relative to the contralateral breast exhibit potential for characterization of pathological response. This initial demonstration of the combined optical approach for chemotherapy monitoring provides incentive for more comprehensive studies in the future and can help power those investigations.

Keywords: diffuse correlation spectroscopy, diffuse optical spectroscopy, neoadjuvant chemotherapy, chemotherapy monitoring, breast cancer imaging, tumor blood flow, tumor metabolism

(Some figures may appear in colour only in the online journal)

Introduction

Neoadjuvant chemotherapy (NAC) is an important treatment method for breast cancer. The approach permits increased conservation of breast tissue during tumor resection and can reduce the need for axillary node surgery and treatment (Sledge *et al* 2014). Furthermore, pathologic complete response (pCR) to NAC, defined as no residual invasive tumor in the resected tissue, has been shown to be correlated with improved patient survival rate compared to incomplete or non-responders (Rastogi *et al* 2008, Esserman *et al* 2012). Importantly, reliable prediction of lesion response at an earlier time point in the chemotherapy would enable physicians to optimize the treatment regimen and avoid unnecessary therapy doses, reduce tissue damage, and improve patient outcomes. In practice, NAC response is evaluated primarily with physical exams, mammography, and ultrasound. These methods, however, are limited as predictors of pCR (Feldman *et al* 1986, Helvie *et al* 1996, Vinnicombe *et al* 1996). By contrast, magnetic resonance imaging (MRI) provides better correlation with pathology than mammography or ultrasound (Yeh *et al* 2005), and functional monitoring techniques offer significantly improved correlation with response relative to structural imaging methods. Magnetic resonance spectroscopy (MRS) (Meisamy *et al* 2004), contrast-enhanced MRI (Hylton *et al* 2012), and positron emission tomography (PET) (Mankoff *et al* 2003, McDermott *et al* 2007), for example, have predictive value with respect to pCR and suggest that metabolism and/or blood flow are correlated with treatment response. Unfortunately, MRI, MRS, and PET all suffer from logistical limitations which limit their viability for serial monitoring of therapy progression in patients undergoing chemotherapy, including high-cost, the use of exogenous contrast agents, and the added issue of ionizing radiation for PET. Thus the present contribution explores the utility of optical chemotherapy monitoring.

Briefly, diffuse optical techniques measure functional hemodynamic properties with non-ionizing near-infrared (NIR) radiation and can be used continuously at the bedside at relatively low cost. The technology is well positioned to predict treatment outcome using repeated measurements throughout the course of therapy (Tromberg *et al* 2008, O'Sullivan *et al* 2012). Specifically, diffuse optical spectroscopic imaging (DOSI) and tomography (DOT) probe deeply into tissue and enable determination of tissue optical absorption (μ_a) and reduced optical scattering coefficients (μ'_s), as well as oxygenated (HbO) and deoxygenated (Hb) hemoglobin concentration and tissue oxygen saturation (StO₂) (Leff *et al* 2008). These reconstructed quantities have been shown to discriminate between malignant and healthy tissue in the breast (Srinivasan *et al* 2005, Spinelli *et al* 2005, Cerussi *et al* 2006, Choe *et al* 2009, Wang *et al* 2010, Fang *et al* 2011, Mastanduno *et al* 2014). Importantly, several studies have employed DOSI techniques to investigate functional changes in malignant tissue over the course of NAC

and have correlated these changes with the patients' responses to treatment (Choe *et al* 2005, Tromberg *et al* 2005, Zhou *et al* 2007, Cerussi *et al* 2007, Zhu *et al* 2008, Jiang *et al* 2009, Soliman *et al* 2010, Cerussi *et al* 2011, Roblyer *et al* 2011, Falou *et al* 2012, Ueda *et al* 2012, Choe and Durduran 2012, Busch *et al* 2013a, Tromberg *et al* 2016, Sajjadi *et al* 2017). The present paper is focused on another diffuse optical technique, diffuse correlation spectroscopy (DCS), which utilizes the temporal fluctuations of detected light intensity to probe microvasculature blood flow in deep tissue (Durduran *et al* 2010). The blood flow index (BFI) ($\text{cm}^2 \text{s}^{-1}$) measured by DCS has been validated in humans against numerous gold-standard techniques (Mesquita *et al* 2011), including transcranial Doppler ultrasound (Buckley *et al* 2009), phase-encoded velocity mapping MRI (Buckley *et al* 2012, Jain *et al* 2014), and xenon-enhanced computed tomography (Kim *et al* 2010). DCS has also been used to characterize hemodynamic properties of normal and malignant human breast tissue (Durduran *et al* 2005, Zhou *et al* 2007, Yu 2012, Busch *et al* 2014, Choe *et al* 2014), to investigate blood flow in the early stages of NAC (Zhou *et al* 2007), and to longitudinally explore whole chemotherapy regimens in a murine model (Ramirez *et al* 2016).

The combined use of DOSI and DCS performed herein for NAC monitoring provides several benefits. First, absolute μ_a and μ'_s values derived by DOSI constrain DCS blood flow fitting and thus reduce cross-talk between changes in optical and blood flow parameters (Irwin *et al* 2011, Farzam and Durduran 2015, Yazdi *et al* 2017). Additionally, the combination of StO_2 , measured by DOSI, with BFI, measured by DCS, permits investigation of oxygen metabolism in malignant tissue; oxygen metabolism is a comparatively new biomarker for chemotherapy response that could enable direct comparison of optical diagnostics to other imaging modalities such as FDG-PET. In this study, four patients enrolled in an ACRIN clinical trial (Tromberg *et al* 2016) were monitored longitudinally using both DCS and DOSI throughout their NAC regimen. The blood flow data in tumor and healthy breast tissue was then analyzed to investigate potential hemodynamic differences between responders and non-responders. Previous studies have used combinations of DCS and DOS instrumentation to monitor breast tumors (Durduran *et al* 2005, Zhou *et al* 2007, Choe *et al* 2014, Yazdi *et al* 2017) and to monitor head and neck tumors (Sunar *et al* 2006, Irwin *et al* 2011), but to our knowledge, this work is the first investigation to use DCS to measure blood flow throughout the course of NAC in humans with breast cancer and the first to correlate DCS hemodynamic properties with pCR and treatment in humans. Our pilot measurements suggest that DCS-derived blood flow parameters are correlated with pCR.

Methods

For this study, four breast cancer patients were imaged at the University of Pennsylvania using both the DOSI instrument developed at the University of California Irvine as part of the ACRIN 6691 study (Tromberg *et al* 2016) and a DCS system developed at the University of Pennsylvania. The subjects were females between the ages of 31 and 65 with biopsy-confirmed invasive carcinomas of at least 2 cm in diameter along the largest axis. The subjects underwent an NAC regimen prior to surgery. All four subjects received either Doxorubicin/Cyclophosphamide, Paclitaxel, or a combination of both within the course of NAC treatment; in addition, hormone receptor positive subjects were given hormone therapy. The chemotherapy regimen was determined by each subject's physician and was not controlled for in this study. Here, pCR was defined as no residual invasive carcinoma, as determined by post-surgery pathology reports.

The custom-built DCS instrumentation used in this study is described elsewhere (Durduran 2004). Briefly, light from a continuous wave, long-coherence length (>5 m), 785 nm laser (DL785-100-30, CrystaLaser, Reno, Nevada) with a maximum power of 100 mW attenuated to within ANSI power limits and coupled to a multimode fiber (200 μm core/0.22NA, 4 m in length, OZ Optics, Ontario, Canada) illuminated the breast tissue. A single-mode detection fiber (5 μm mode field diameter/0.13NA, 4 m in length, OZ Optics, Ontario, Canada) couples diffusive light emerging from the tissue to a single photon counting avalanche photodiode (SPCM-AQ4C, Excelitas, Quebec, Canada) operating in photon counting mode. The source and detector probe was placed on the tissue with minimal pressure to prevent significant pressure-induced changes in blood flow. The photodiode's collected light intensity at time t ($I(t)$) was sent to a multiple- τ hardware correlator (Flex02OEM4ch, Correlator.com, New Jersey) for computation of the normalized intensity autocorrelation function in real time, i.e. computation of $g_2(\tau) \equiv \langle I(t)I(t+\tau) \rangle / \langle I(t) \rangle^2$. Here, the angular brackets, $\langle \rangle$, represent time-averages over an interval of 2.5 s. A semi-infinite homogeneous tissue model is employed to derive a DCS blood flow index, BFI, from the temporal decay of $g_2(\tau)$. We note that multi-layer models for DCS fitting have also been explored to reduce the signal contamination from blood flow in the superficial skin/skull layer of the head (Jaillon *et al* 2006, Shang and Yu 2014, Baker *et al* 2015). However, in this study, the superficial (skin) layer was very thin in comparison to the source-detector separation. Moreover, the study did not incorporate multiple source-detector separations nor *a priori* anatomical knowledge of the superficial layer thickness. Therefore, we chose to utilize the simple semi-infinite model as both the best fit to the anatomy and to avoid unverified assumptions.

Formally, the normalized autocorrelation function of the electric field ($\mathbf{E}(t)$), i.e. $g_1(\tau) \equiv \langle \mathbf{E}^*(t) \cdot \mathbf{E}(t+\tau) \rangle / \langle I(t) \rangle$, is obtained from the measured normalized intensity autocorrelation function via the Siegert relation (Lemieux and Durian 1999). $g_1(\tau)$ is in turn modeled by the semi-infinite homogeneous medium solution to the correlation diffusion equation, which depends on the underlying tissue BFI, μ_a , and μ'_s (Boas *et al* 1995, Boas and Yodh 1997). The semi-infinite correlation diffusion solution is fit to $g_1(\tau)$ using a nonlinear minimization algorithm, and an estimate of BFI is obtained from the fit (Boas and Yodh 1997, Durduran *et al* 2010).

The spatio-temporally co-registered DOSI instrument combines multispectral frequency-domain and broadband imaging to measure absolute μ_a , μ'_s , and the tissue concentrations of oxygenated hemoglobin (HbO), deoxygenated hemoglobin (Hb), water, and lipid. The combination of these chromophores permits calculation of tissue total hemoglobin concentration (Hb_T) and tissue oxygen saturation (StO₂). A full description of this instrument and imaging technique has been published (Bevilacqua *et al* 2000).

Each subject was imaged at four time points throughout the course of treatment (see figure 1). The first (Baseline) measurement occurred prior to the subject's first chemotherapy treatment. The second measurement, which hereafter will be referred to as the Early measurement, was performed between 5 and 10 d after the first chemotherapy treatment. This time period was chosen in order to avoid the so-called oxyhemoglobin flare that has been found to occur immediately after chemotherapy treatment (Zhou *et al* 2007, Roblyer *et al* 2011). A third measurement was made at the midpoint of the therapy regimen (Midpoint), and a final measurement (Final) was made at the conclusion of the regimen, prior to surgical intervention.

During the Baseline measurement, a 10×10 grid of points with 10 mm spacing between adjacent points was marked on the subject's skin. The location of this grid was chosen to encompass the entire extent of the lesion and to include the surrounding healthy tissue. The location of and extent of the lesion was derived from an ultrasound image. The measurement grid was then recorded using a transparency, so that its location could be accurately replicated

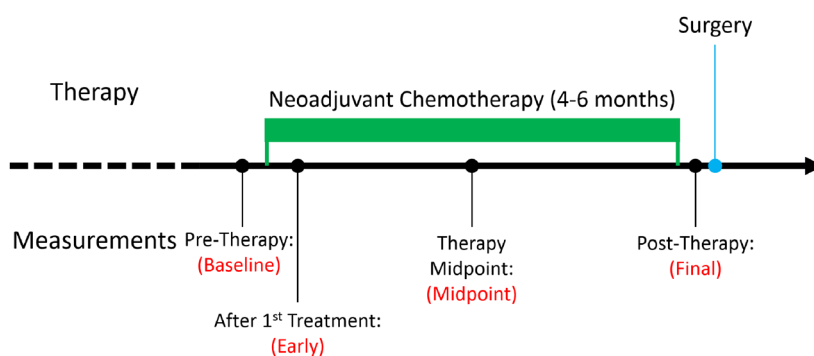


Figure 1. Timeline of optical monitoring during NAC. Each subject underwent NAC for a period of 4 to 6 months prior to tumor resection surgery. DCS and DOSI measurements were made at four different time points throughout this process: (1) Baseline—prior to the administration of the first dose of chemotherapy. (2) Early—5 to 10 d after the first dose of chemotherapy. (3) Midpoint—at the midpoint of the therapy regimen. (4) Final—at least 7 d after the final dose of therapy and prior to the tumor resection surgery.

during future measurements. A mirrored 10×10 grid of points was also marked on the contralateral breast. DOSI data was recorded at each of the points on both grids, thereby providing images of the underlying tissue optical properties and chromophore concentrations, as well as absolute optical properties at each point.

DCS data was collected along a single line of points (~ 10 points) on each grid. This line was chosen to traverse both lesion and non-lesion tissue on the tumor-bearing breast and was mirrored to the same locations on the contralateral breast (see figure 2). The corresponding DOSI absolute μ_a and μ'_s calculated at each point were utilized as inputs in the fitting algorithm for the DCS BFI. The DCS BFI was also calculated using a single set of assumed μ_a and μ'_s values that most closely fit our DOSI-measured optical property data. The error in the BFI between these two methods was then calculated as a function of the μ_a and μ'_s errors in order to determine the effect of inaccurate optical properties on the BFI calculation.

Finally, as noted above, the combination of DCS blood flow measurements (BFI) with DOSI tissue oxygen saturation (StO_2) measurements permits investigation of tissue oxygen metabolism. Using the Fick principle, the mammary metabolic rate of oxygen consumption (MMRO_2) can be given by equation (1) (Zhou *et al* 2007, Busch *et al* 2013b)

$$\text{MMRO}_2 = \gamma(1 - \text{StO}_2)\text{BFI}. \quad (1)$$

Here, $\gamma \equiv \kappa \frac{\text{Hb}_v/\text{Hb}_{T,v}}{\text{Hb}/\text{Hb}_T}$. It depends on the ratio of deoxyhemoglobin to total hemoglobin concentration in the venous vascular compartment (i.e. $\text{Hb}_v/\text{Hb}_{T,v}$) relative to the ratio of deoxyhemoglobin to total hemoglobin in all tissue (e.g. as determined by DOSI tissue measurements); it also depends on the proportionality coefficient between BFI and absolute blood flow, i.e. κ . Equation (1) assumes that the arterial oxygen saturation is unity. In both this data set and in past studies (Zhou *et al* 2007, Busch *et al* 2013b), γ is unknown because it is not readily feasible to separate the venous compartment contribution to the optical signal from that of the arterial and capillary contributions and because the DCS-measured BFI ($\text{cm}^2 \text{s}^{-1}$) has not been calibrated to obtain κ . Thus, instead of estimating absolute MMRO_2 , in this work we derive the relative tumor-normal (T/N) oxygen metabolism ratio, $\text{rMMRO}_{2(T/N)}$, and temporal changes in tumor oxygen metabolism relative to the Baseline time point (see figure 1), rMMRO_{2B} .

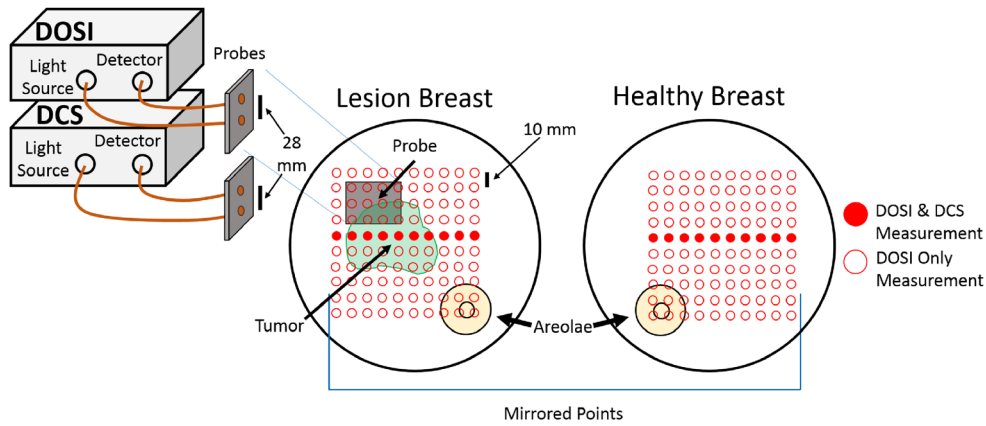


Figure 2. Schematic of the DOSI and DCS measurements. Left: DCS and DOSI instruments and probes. Right: A 10×10 grid of DOSI measurements were made on each of the subject's breasts. The location of the 10×10 grid was chosen to encompass the entire lesion and was then recorded on a transparency along with physiological landmarks such as moles, freckles, and the areola. This transparency allowed for a mirrored grid of points to be measured on the contralateral (healthy) breast. DCS measurements were made at a single line of 10 grid points that completely traversed the lesion and the 10 corresponding points on the contralateral breast.

The relative tumor-normal oxygen metabolism ratio is the oxygen metabolism of a point over the tumor divided by the oxygen metabolism at the corresponding position on the contralateral breast. It is calculated via

$$\text{rMMRO}_{2(T/N)} \approx \left(\frac{1 - \text{StO}_{2T}}{1 - \text{StO}_{2N}} \right) \left(\frac{\text{BFI}_T}{\text{BFI}_N} \right). \quad (2)$$

Here, StO_{2T} and BFI_T represent StO_2 and BFI measurements made at a spatial location within the tumor region (see figure 2) at the time point of interest during NAC treatment (see figure 1), and StO_{2N} and BFI_N are StO_2 and BFI measurements made at the corresponding spatial location on the contralateral breast. Equation (2) assumes that γ in equation (1) is the same for both breasts.

Similarly, temporal relative changes in tumor oxygen metabolism are calculated via

$$\text{rMMRO}_{2B} \approx \left(\frac{1 - \text{StO}_{2T}}{1 - \text{StO}_{2T,B}} \right) \left(\frac{\text{BFI}_T}{\text{BFI}_{T,B}} \right), \quad (3)$$

where StO_{2T} and BFI_T are defined as in equation (2) and $\text{StO}_{2T,B}$ and $\text{BFI}_{T,B}$ explicitly denote StO_{2T} and BFI_T for the Baseline time point (see figure 1). Equation (3) assumes that γ in equation (1) remains constant for all measurement time points during NAC treatment.

We note that while this approach is a sensible first approximation, the assumption of constant γ is not verified, and its verification would require research into the microcirculation of malignant and healthy tissue that is beyond the scope of this study.

Results

All four of the measured subjects were diagnosed with biopsy-confirmed invasive ductal carcinomas. Two of the four subjects achieved pCR as determined by the post-surgery pathology report. One of the complete responders was pre-menopausal and one was post-menopausal.

Similarly, one of the non-pCR subjects was pre-menopausal while the other was post-menopausal. Across the four subjects, 36 total spatial points were measured on the subjects' lesion-bearing breasts, and 40 total spatial points were measured on the subjects' contralateral breasts (~10 spatial points per subject per breast) for each of the four longitudinal time points. Of the 36 total spatial points on the ipsilateral breast, 22 points were directly above the ultrasound-confirmed location of the lesion.

The data was divided into contralateral (healthy) and lesion-bearing breast data for each subject and then grouped based on response to chemotherapy (pCR and non-pCR). The points on the lesion breast were further divided into points directly over the tumor and points in the nominally normal tissue surrounding the tumor. The blood flow at the non-tumor points on the lesion-bearing breast tended to resemble the blood flow in the healthy breast and thus will not be shown in the figures. For the responder group (pCR), 11 spatial points were measured in the tumor region (5 on one subject, 6 on the other subject) and 19 spatial points were measured on the healthy breast (9 on one subject, 10 on the other subject) across the two subjects. The non-responder group (non-pCR) had 11 spatial points in the tumor region (6 on one subject, 5 on the other subject) and 21 spatial points on the healthy breast (10 on one subject, 11 on the other subject). Note, due to the small sample size of our data set, herein we explore potentially interesting distinctions that are suggested by the data, but we do not attempt to claim statistically significant differences between the responders and non-responders.

Figure 3 shows the DCS BFI measurements at each of the four longitudinal time points for both healthy breast and tumor tissue. Notice first that the BFI is lower in responders compared to non-responders. This distinction exists at all four temporal points, but the distinction becomes more pronounced at the Midpoint and Final time points of the chemotherapy regimen, at which time, the difference between the responders' and non-responders' tumor blood flow is apparent despite clear intra-subject spatial heterogeneity in blood flow. At these points the responders' tumor BFI begins to resemble the BFI in the responders' healthy breast tissue while the non-responders' tumor BFI remains elevated relative to the non-responders' normal tissue. Furthermore, the potential for differentiation can be seen in both the tumor-bearing and healthy breasts, indicating that the response, or lack of response, to chemotherapy may be a systemic effect.

We also explored BFI in the lesion-bearing breast normalized to BFI in the contralateral breast. This relative tumor-to-normal (T/N) blood flow index ($rBFI_{(T/N)}$) is analogous to the T/N ratios of StO_2 and Hb_T concentration, among other markers, explored in the ACRIN 6691 study (Tromberg *et al* 2016). The $rBFI_{(T/N)}$ at each time point for both responders and non-responders is shown in figure 4. Interestingly, at the Midpoint measurement, the responders' $rBFI_{T/N}$ approaches 1 (mean $rBFI_{T/N} = 1.34$ across the responders' 11 measured spatial points) while the non-responders' tumor blood flow remains elevated relative to normal tissue (mean $rBFI_{T/N} = 2.65$ across the non-responders' 11 measured spatial points). Additionally, differences between responders and non-responders can be seen in the fractional change of average $rBFI_{(T/N)}$ between the Baseline and Early measurements (pCR = +70.9%, non-pCR = -42.5%) and between the Early and Midpoint measurements (pCR = -63.6%, non-pCR = +3.5%). Thus, though we do not have a sufficiently large sample size to draw definitive conclusions, these observations represent promising and physiologically suggestive results that strongly indicate further investigation is warranted.

The data also demonstrates the benefit of including the DOSI measurements of absolute μ_a and μ'_s as inputs in the DCS fitting algorithm for calculating BFI. Without the DOSI measurement, optical properties must be assumed based on literature values. This assumption can be problematic due to the relatively large observed inter- and intra-subject heterogeneity of breast tissue optical properties (see figure 5). To characterize this effect, we employed this data set

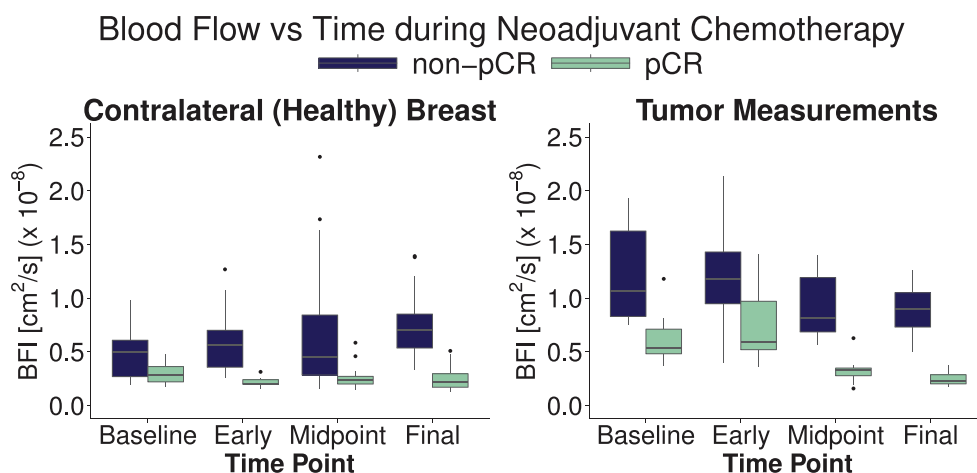


Figure 3. Boxplots of the DCS blood flow index (BFI) ($\text{cm}^2 \text{s}^{-1}$) measurements made in healthy tissue (left panel) and tumor tissue (right panel) at each measurement time point during the NAC treatment (see figure 1). The two boxplots for each measurement time point correspond to the measurements in subjects with pathologic complete response (pCR) ($n = 19$ points in healthy tissue and $n = 11$ points in tumor tissue) and with non-pathologic complete response (non-pCR) ($n = 21$ points in healthy tissue and $n = 11$ points in tumor tissue). In both healthy and tumor tissue, the absolute BFI is lower for responders than for non-responders. Furthermore, the separation between responders and non-responders is larger at the Midpoint and Final measurements. At these points, the tumor BFI for responders is approaching that of the responders' normal tissue, potentially indicating the efficacy of the chemotherapy. The hinges of the boxplots (here and in all other figures) are the first and third quartiles of the data. Lines above and below the boxplot indicate the farthest measurements within $1.5 \times$ the interquartile range. Measurements beyond $1.5 \times$ the interquartile range are plotted as dots.

and compared the BFI values calculated using DOSI-measured optical properties to $\text{BFI}_{\text{assumed}}$ values calculated using constant (assumed) optical properties. Here we chose the assumed optical properties that provided the best overall agreement between $\text{BFI}_{\text{assumed}}$ and BFI, i.e. $\mu_a = 0.0045 \text{ mm}^{-1}$ and $\mu'_s = 0.85 \text{ mm}^{-1}$. Figure 6 demonstrates the extent to which deviations between assumed and measured optical properties affect the calculated BFI.

We see, for example, that a percent error of 50% in μ_a produces an $\sim 20\%$ change in BFI, while a percent error of 25% in μ'_s produces a 25–45% change in BFI, which is consistent with the errors due to optical property offsets seen in a previous study (Irwin *et al* 2011). These variations are within typical intra-subject optical property ranges, as evidenced by figure 5, particularly in the lesion-bearing breast. We also found that when using assumed optical properties, approximately 75% of the measured BFI values are at least 10% away from their true value and approximately 51% of the measured BFI values are at least 20% away from their true value (see figure 6-Inset).

The effects of optical property errors on the relative BFI parameters (i.e. $\text{rBFI}_{(TN)}$) is less severe but still significant, especially for scattering errors. In figure 4, each blood flow index boxplot for non-responders, which represents $\text{rBFI}_{(TN)}$ at a given longitudinal time point, has a 35% larger normalized standard deviation (on average) when assumed optical properties are used instead of DOSI-measured properties. We observe no significant difference in the normalized standard deviation for the responders in this data set because the responders' measured optical properties are, on average, less heterogeneous than the non-responders', and the responders' μ'_s values, which have a larger effect on the BFI calculation than μ_a (see figure 6),

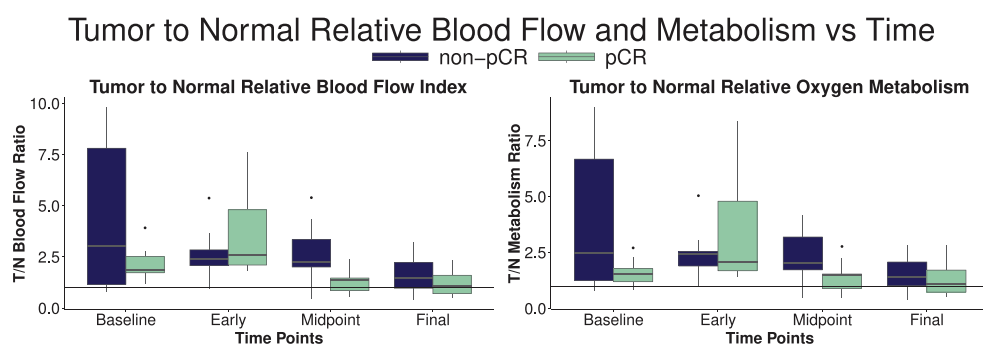


Figure 4. Tumor to normal blood flow and oxygen metabolism measurements. Left: box plots of blood flow in the tumor tissue normalized to the flow in the contralateral (healthy) breast ($rBFI_{(T/N)}$) at each time point separated into responders (pCR) and non-responders (non-pCR). The responder group experiences an increase in $rBFI_{(T/N)}$ between the Baseline and Early measurements, followed by a steep decline in $rBFI_{(T/N)}$ between the Early and Midpoint measurements. The non-responder group experiences a slight decrease in $rBFI_{(T/N)}$ between the Baseline and Early measurements but no change between the Early and Midpoint measurements. At the Midpoint measurement, the responder group has a mean $rBFI_{(T/N)}$ of 1.34 ($n = 11$ spatial points) while the non-responder group has a mean $rBFI_{(T/N)}$ of 2.65 ($n = 11$ spatial points). This indicates that the responders' blood flow in the lesion is approaching normal levels by the midpoint of therapy while the non-responders' is still elevated. Right: box plots of oxygen metabolism in the tumor tissue normalized to the oxygen metabolism in the contralateral (healthy) breast ($rMMRO_{2(T/N)}$). Note that $rMMRO_{2(T/N)}$ follows a similar trend to the $rBFI_{(T/N)}$ for responders and non-responders due to the relatively small difference in StO_2 between tumor and normal tissue.

are clustered around the assumed μ'_s value (see figure 5). The observed heterogeneity in optical properties suggests that in future studies, subject-specific measurement of optical properties is important, and therefore, the combination of DOSI and DCS will likely be necessary for maximizing the utility of DCS blood flow as an early marker of NAC treatment efficacy.

Finally, we investigated the combination of StO_2 measurements from the DOSI data and BFI measurements with DCS to calculate the T/N ratio of oxygen metabolism, $rMMRO_{2(T/N)}$ (equation (2)). We found that $rMMRO_{2(T/N)}$ closely tracks $rBFI_{(T/N)}$ because of the relatively small difference in StO_2 between tumor and normal tissue (see figure 4). To further explore the utility of the oxygen metabolism measurement, we also calculated the Baseline-normalized blood flow index, $rBFI_B$, oxygen saturation $rStO_{2B}$, and oxygen metabolism, $rMMRO_{2B}$ (equation (3)). Figure 7 provides a case study comparing these three quantities for a single subject, along with potential explanations for the findings.

Discussion

The results we have presented represent an important step towards the use of DCS blood flow (BFI) as a biomarker of NAC response. In the long term, the ability to accurately quantify BFI in multiple subjects and at different spatial locations across optically heterogeneous breasts will be an important factor in determining the utility of DCS blood flow as a predictor of a patient's response to treatment. The incorporation of absolute tissue optical properties determined by DOSI into the DCS blood flow calculation improves the accuracy of blood flow measurements by isolating the effects of actual blood flow changes from concurrent changes in optical properties.

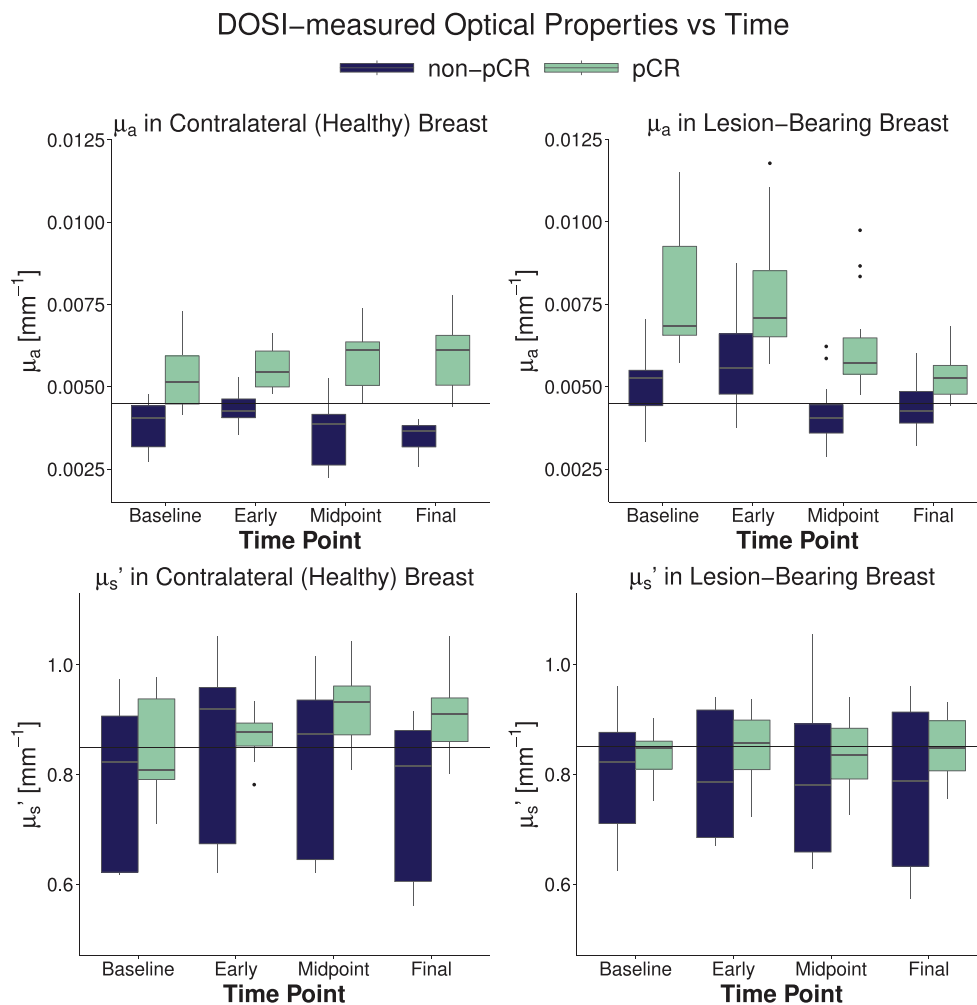


Figure 5. DOSI-measured optical properties at 785 nm wavelength. Boxplots of μ_a and μ_s' in both breasts are plotted for responders and non-responders across all four time points. The responders' data set consists of 15 spatial points measured on the lesion-bearing breasts and 19 spatial points measured on the healthy breasts. The non-responders' data set consists of 21 spatial points on the lesion-bearing breasts and 21 spatial points on the healthy breasts. The horizontal lines on each graph indicate the assumed optical properties ($\mu_a = 0.0045 \text{ mm}^{-1}$; $\mu_s' = 0.85 \text{ mm}^{-1}$) used as inputs to the DCS fits for calculation of BFI when the DCS analysis is performed without DOSI data. Note that the responders and non-responders exhibit similar heterogeneity and offset from the assumed values in the μ_a plots. However, the optical properties of the responders are more homogeneous and clustered around the assumed value for the μ_s' plots. This observation explains why the non-responders have a relatively large increase in normalized standard deviation of $\text{rBFI}_{(TN)}$ ($\sim 35\%$) when assumed optical properties are used, while the standard deviation for the responders data is virtually unchanged.

The absolute BFI measurements and the normalized $\text{rBFI}_{(TN)}$ offer interesting possibilities for early differentiation between responders and non-responders. For example, we expect effective chemotherapy treatments to inhibit cell metabolism and/or angiogenesis. Thus, we expect lower blood flow levels in the tumor regions of responders compared to non-responders.

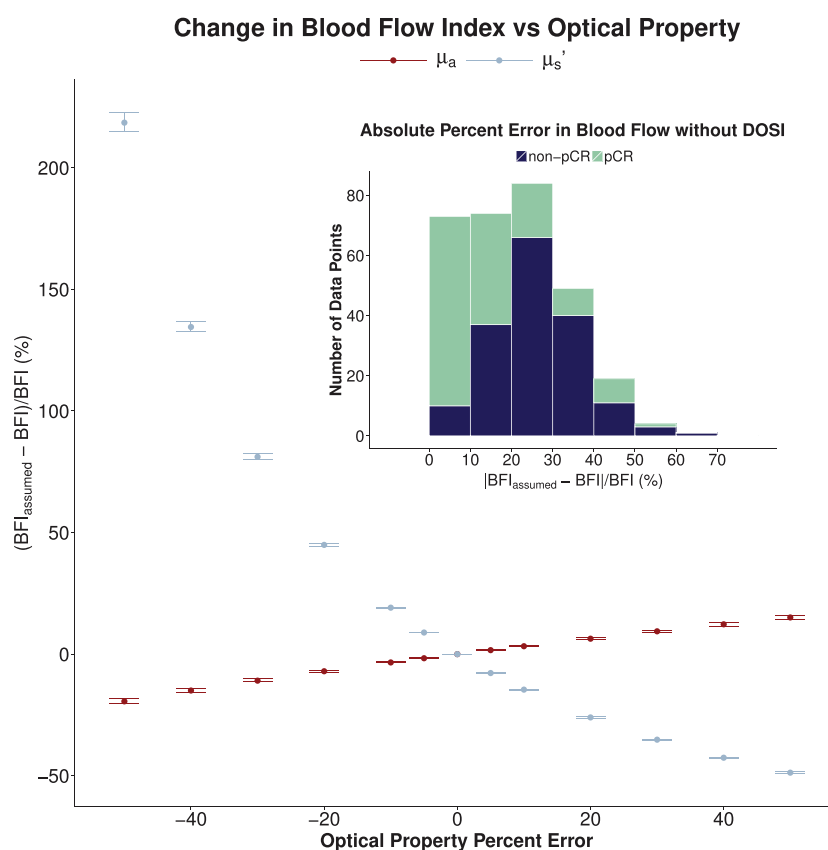


Figure 6. Effect of tissue optical property errors on blood flow index (BFI) calculation. Main: percent error in the calculated absolute BFI (i.e. $100 \times (BFI_{\text{assumed}} - BFI)/BFI$) plotted against the percent error in the assumed μ_a relative to the DOSI-measured value (red curve) and against the percent error in the assumed μ_s' relative to the DOSI-measured value (blue curve). Note that the values on the vertical axis are plotted as mean \pm SD for the data points at each value of the optical property percent error. Clearly, μ_s' errors have a larger effect on the calculated BFI than μ_a errors. Inset: histogram of the error in BFI measurements when using assumed μ_a and μ_s' versus DOSI-measured μ_a and μ_s' across all subjects and time points. Approximately 75% of all points have an error of greater than 10%, 51% of all points have an error of greater than 20%, and 22% of all points have an error of greater than 30%. Also note that the responders generally have less error in the BFI measurements with assumed optical properties than non-responders; this effect is due to a smaller error in the assumed μ_s' for the responders (see figure 5).

The lower levels of absolute BFI and $rBFI_{(TIN)}$ during chemotherapy for responders found in our study are consistent with these expectations, as well as with changes found in previous blood flow studies using FDG-PET (Mankoff *et al* 2003, Avril *et al* 2016) and with the changes in hemoglobin concentration measured in the ACRIN 6691 study (Tromberg *et al* 2016). We caution, however, that the increase in responders' $rBFI_{(TIN)}$ between the Baseline and Early measurements (see figure 4) could potentially correspond to the oxyhemoglobin flare that has previously been observed in NAC responders (Zhou *et al* 2007, Roblyer *et al* 2011) or to particular chemotherapeutic mechanisms that will be discussed later (see figure 7).

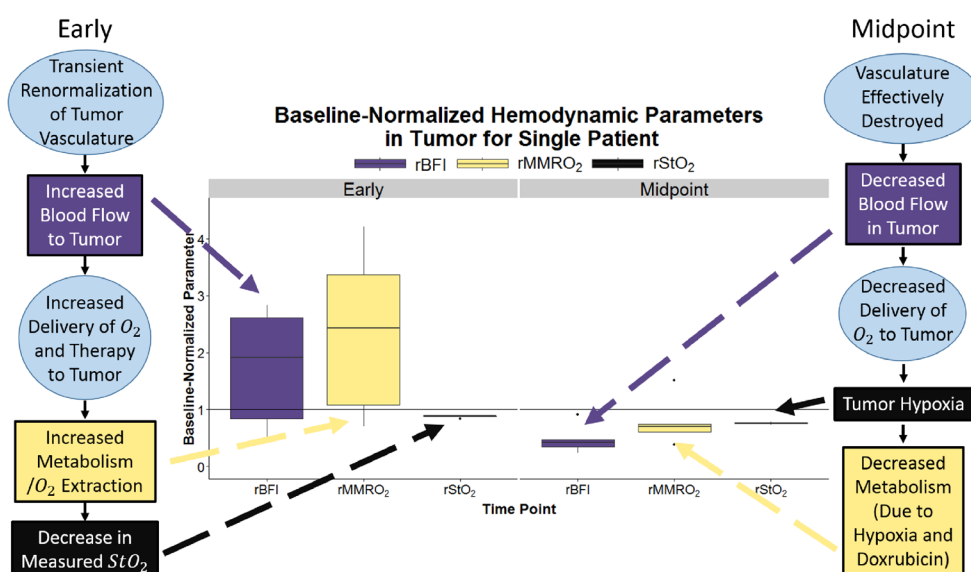


Figure 7. Baseline-normalized hemodynamic parameters during administration of Doxorubicin/Cyclophosphamide treatment for a single subject. Each measured point is normalized to the corresponding spatial point in the Baseline measurement. The flow charts indicate the expected physiological mechanism of the chemotherapy at the given time points. At the Early time point, transient re-normalization of the vasculature leads to increases in both $rBFI_B$ and $rMMRO_{2_B}$. At the Midpoint, the therapy has effectively destroyed the tumor vasculature, which, combined with the cytotoxicity of Doxorubicin, has inhibited cell metabolism, leading to decreased $rBFI_B$ and $rMMRO_{2_B}$, as well as relative tumor hypoxia, i.e. decreased $rStO_{2_B}$. This case study displays the potential of oxygen metabolism measurements from combined DCS/DOSI to track the physiological mechanisms and efficacy of chemotherapy treatment.

Indications of treatment efficacy at the midpoint of treatment or earlier are of particular interest because they could enable oncologists to augment or change an ineffective therapy regimen. At the Midpoint time point in this data set, the average $rBFI_{(T/N)}$ of the responders approaches 1 while the same quantity for the non-responders remains abnormal. This observation suggests that by the treatment midpoint, blood flow in the lesion has begun to resemble that of the normal breast in responders, while the non-responders still have anomalous blood flow. Again, this finding is consistent with both intuition about the efficacy of treatment and with data from the larger ACRIN 6691 DOSI study which indicate that some hemodynamic properties of responders and non-responders are distinguishable by the midpoint of treatment (Tromberg *et al* 2016).

The calculation of T/N oxygen metabolism, $rMMRO_{2(T/N)}$, closely tracks $rBFI_{(T/N)}$ (see figure 4), which is consistent with a relatively small average difference in StO_2 between tumor and normal tissue that is seen in this study and in previous studies (Cerussi *et al* 2006, Choe *et al* 2009, Busch *et al* 2010). However, investigation into $rMMRO_{2(T/N)}$ is still important because the oxygen saturation of tumors is very heterogeneous and dependent on biochemical characteristics and the stage of the cancer (Choe *et al* 2009). Therefore, the tumor StO_2 may vary greatly from the normal StO_2 for a given patient. In that case, $rBFI_{(T/N)}$ alone would not be an accurate marker of metabolism.

One reason to measure oxygen metabolism is that there are potential physiological scenarios wherein blood flow and metabolism measurements could more accurately reflect the

physiological changes in the tumor than measurements of blood flow alone. We performed a case study of a single subject to explore these potential physiological changes (see figure 7). The data correspond to Baseline-normalized $rBFI_B$, $rMMRO_{2B}$, and $rStO_{2B}$ during the administration of a Doxorubicin/Cyclophosphamide treatment regimen. In this case, we observe a transient increase in both blood flow and metabolism in the tumor during the Early time point, which is consistent with blood flow increases seen immediately after the administration of this therapy combination in mouse models (Ramirez *et al* 2016). The initial increase in blood flow is likely due to the transient re-normalization of the tumor vasculature caused by the anti-angiogenic effects of the chemotherapy regimen (Jain 2005). Vascular re-normalization allows for increased oxygen metabolism and enables delivery of therapy to the tumor cells. At the Midpoint measurement, however, $rBFI_B$ and $rMMRO_{2B}$ are depressed, potentially indicating an effective response to treatment in which the Doxorubicin/Cyclophosphamide combination has inhibited cell metabolism and effectively destroyed the tumor vasculature. In contrast, a chemotherapy regimen that primarily disrupts cancer cell metabolism, with little angiogenic inhibition, would likely exhibit more significant changes in measurements of $rMMRO_{2B}$ than in measurements of $rBFI_B$. The combination of DCS and DOSI, along with the subsequent calculation of oxygen metabolism, will enable further exploration of these physiological changes, and their correlation with treatment response, in future optical studies.

The distinctions between the responders and non-responders in both absolute BFI (figure 3) and $rBFI_{TN}$ and $rMMRO_{2(T/N)}$ (figure 4), combined with the fact that these effects are consistent with both expectations about hemodynamics from previous studies and with the expected physiological mechanisms of chemotherapy, provide motivation to further investigate the predictions of DCS measurements during neoadjuvant chemotherapy with a larger sample size. An obvious future direction for this work is to complete a study with a larger subject population that permits more statistically significant differentiation between responders and non-responders, especially at the more clinically valuable Early and Midpoint measurements. Over the course of this future study, several changes could also be made to the measurement protocol to collect additional, useful information. First, more spatial points could be collected on each breast to enable diffuse correlation tomography (DCT) blood flow image reconstruction. In this case, DOSI measurements could also be used to spatially constrain the DCT inverse problem. This augmentation could improve blood flow index quantification in the lesion tissue, in the nominally healthy tissue of the lesion-bearing breast, and in the contralateral breast. Finally, it appears valuable to explore techniques for determining absolute oxygen metabolism ($MMRO_2$) instead of relative oxygen metabolism ($rMMRO_{2(T/N)}$) by isolating the venous contribution to the optical signal. Advances along these lines would enable the DCS/DOSI combination to potentially track systemic metabolic changes in addition to the relative changes between healthy and lesion-bearing breasts.

Conclusion

We presented the first pilot study using diffuse correlation spectroscopy to monitor blood flow throughout the course of neoadjuvant chemotherapy in a human clinical trial and the first investigation into the potential correlation between DCS-measured blood flow index and NAC response. We demonstrated the value of combining DCS with diffuse optical spectroscopic imaging, both to constrain the DCS fitting and for calculating information about oxygen metabolism. Clearly, DCS and DOSI are attractive modalities for the monitoring of response to treatment due to their sensitivity to functional hemodynamic properties, as well as their portability, their use of non-ionizing radiation, and their relatively low cost. The results

suggest the existence of an interesting correlation between pathologic complete response to NAC and both lower absolute BFI and lower relative BFI between the tumor and normal tissue at the midpoint of the chemotherapy regimen. The calculation of oxygen metabolism using the combined DOSI and DCS data also presented an interesting opportunity to more accurately explore the physiological mechanisms and efficacy of chemotherapy. Finally, these pilot results provide data for powering future comprehensive clinical studies which aim to correlate blood flow, oxygen metabolism, and oxygen dynamics with pCR.

Acknowledgments

Funding for this study was provided through grants from the American College of Radiology Imaging Network, which receives funding from the National Cancer Institute (U01-CA079778, U01-CA080098), the National Institutes of Health (P41-EB015893, R01-NS060653, R01-EB002109, R01-CA142989, P41-EB015890, U54-CA136400, T32-HL007915, R01-NS072338, R01-NS082309-01A1), the Thrasher Research Foundation, the June and Steve Wolfson Family Foundation, and the Susan G Komen for the Cure Postdoctoral Fellowship. The authors would like to thank Regine Choe for many helpful discussions and Madeline Winters, Sarah Grundy, Jennifer Lynch, Erin Buckley, Ellen Foster, and Michelle Wong for the recruitment of subjects and/or help with data collection.

B J Tromberg reports receiving a commercial research grant from LG Electronics, has ownership interest (including patents) in intellectual property related to breast imaging assigned to UC Regents, and is a consultant/advisory board member for Hamamatsu Photonics. D R Busch, W B Baker, and A G Yodh have two pending patent applications and A G Yodh has two other patents relevant to this work (United States patents 8,082,015 and 6,076,010). The other authors have indicated no financial conflicts of interest.

References

- Avril S, Muzic R F, Plecha D, Traughber B J, Vinayak S and Avril N 2016 18f-fdg pet/ct for monitoring of treatment response in breast cancer *J. Nucl. Med.* **57** 34S–9S
- Baker W B *et al* 2015 Pressure modulation algorithm to separate cerebral hemodynamic signals from extracerebral artifacts *Neurophotonics* **2** 035004
- Bevilacqua F, Berger A J, Cerussi A E, Jakubowski D and Tromberg B J 2000 Broadband absorption spectroscopy in turbid media by combined frequency-domain and steady-state methods *Appl. Opt.* **39** 6498–507
- Boas D A and Yodh A G 1997 Spatially varying dynamical properties of turbid media probed with diffusing temporal light correlation *J. Opt. Soc. Am. A* **14** 192–215
- Boas D A, Campbell L E and Yodh A G 1995 Scattering and imaging with diffusing temporal field correlations *Phys. Rev. Lett.* **75** 1855–58
- Buckley E M *et al* 2009 Cerebral hemodynamics in preterm infants during positional intervention measured with diffuse correlation spectroscopy and transcranial doppler ultrasound *Opt. Express* **17** 12571–81
- Buckley E M *et al* 2012 Validation of diffuse correlation spectroscopic measurement of cerebral blood flow using phase-encoded velocity mapping magnetic resonance imaging *J. Biomed. Opt.* **17** 037007
- Busch D R, Choe R, Durduran T and Yodh A G 2013b Towards non-invasive characterization of breast cancer and cancer metabolism with diffuse optics *PET Clin.* **8** 345–65
- Busch D R, Choe R, Durduran T, Friedman D H, Baker W B, Maidment A D, Rosen M A, Schnall M D and Yodh A G 2014 Blood flow reduction in breast tissue due to mammographic compression *Acad Radiol.* **21** 151–61

- Busch D R *et al* 2013a Optical malignancy parameters for monitoring progression of breast neoadjuvant chemotherapy *Biomed. Opt. Express* **4** 105–21
- Busch D R *et al* 2010 Computer aided automatic detection of malignant lesions in diffuse optical mammography *Med. Phys.* **37** 1840–9
- Cerussi A E, Tanamai V W, Hsiang D, Butler J, Mehta R S and Tromberg B J 2011 Diffuse optical spectroscopic imaging correlates with final pathological response in breast cancer neoadjuvant chemotherapy *Phil. Trans. A* **369** 4512–30
- Cerussi A, Hsiang D, Shah N, Mehta R, Durkin A, Butler J and Tromberg B J 2007 Predicting response to breast cancer neoadjuvant chemotherapy using diffuse optical spectroscopy *Proc. Natl Acad. Sci.* **104** 4014–9
- Cerussi A, Shah N, Hsiang D, Durkin A, Butler J and Tromberg B J 2006 *In vivo* absorption, scattering, and physiologic properties of 58 malignant breast tumors determined by broadband diffuse optical spectroscopy *J. Biomed. Opt.* **11** 044005
- Choe R and Durduran T 2012 Diffuse optical monitoring of the neoadjuvant breast cancer therapy *IEEE J. Sel. Top. Quantum Electron.* **18** 1367–86
- Choe R *et al* 2005 Diffuse optical tomography of breast cancer during neoadjuvant chemotherapy: a case study with comparison to mri *Med. Phys.* **32** 1128–39
- Choe R *et al* 2009 Differentiation of benign and malignant breast tumors by *in vivo* three-dimensional parallel-plate diffuse optical tomography *J. Biomed. Opt.* **14** 024020
- Choe R *et al* 2014 Optically measured microvascular blood flow contrast of malignant breast tumors *PLoS One* **9** e99683
- Durduran T 2004 Non-invasive measurements of tissue hemodynamics with hybrid diffuse optical methods *PhD Thesis* University of Pennsylvania
- Durduran T, Choe R, Baker W B and Yodh A G 2010 Diffuse optics for tissue monitoring and tomography *Rep. Prog. Phys.* **73** 076701
- Durduran T, Choe R, Yu G, Zhou C, Tchou J C, Czerniecki B J and Yodh A G 2005 Diffuse optical measurement of blood flow in breast tumors *Opt. Lett.* **30** 2915–7
- Esserman L J *et al* 2012 Pathologic complete response predicts recurrence-free survival more effectively by cancer subset: results from the i-spy 1 trial-calgb 150007/150012, acrin 6657 *J. Clin. Oncol.* **30** 3242–9
- Falou O *et al* 2012 Diffuse optical spectroscopy evaluation of treatment response in women with locally advanced breast cancer receiving neoadjuvant chemotherapy *Trans. Oncol.* **5** 238–46
- Fang Q, Selb J, Carp S A, Boverman G, Miller E L, Brooks D H, Moore R H, Kopans D B and Boas D A 2011 Combined optical and x-ray tomosynthesis breast imaging *Radiology* **258** 89–97
- Farzam P and Durduran T 2015 Multidistance diffuse correlation spectroscopy for simultaneous estimation of blood flow index and optical properties *J. Biomed. Opt.* **20** 55001
- Feldman L D, Hortobagyi G N, Buzdar A U, Ames F C and Blumenschein G R 1986 Pathological assessment of response to induction chemotherapy in breast cancer *Cancer Res.* **46** 2578–81
- Helvie M A, Joynt L K, Cody R L, Pierce L J, Adler D D and Merajver S D 1996 Locally advanced breast carcinoma: accuracy of mammography versus clinical examination in the prediction of residual disease after chemotherapy *Radiology* **198** 327–32
- Hylton N M *et al* 2012 Locally advanced breast cancer: mr imaging for prediction of response to neoadjuvant chemotherapy—results from acrin 6657/i-spy trial *Radiology* **263** 663–72
- Irwin D, Dong L, Shang Y, Cheng R, Kudrimoti M, Stevens S D and Yu G 2011 Influences of tissue absorption and scattering on diffuse correlation spectroscopy blood flow measurements *Biomed. Opt. Express* **2** 1969–85
- Jaillon F, Skipetrov S E, Li J, Dietsche G, Maret G and Gisler T 2006 Diffusing-wave spectroscopy from head-like tissue phantoms: influence of a non-scattering layer *Opt. Express* **14** 10181–94
- Jain R K 2005 Normalization of tumor vasculature: an emerging concept in antiangiogenic therapy *Science* **307** 58–62
- Jain V *et al* 2014 Cerebral oxygen metabolism in neonates with congenital heart disease quantified by mri and optics *J. Cerebral Blood Flow Metab.* **34** 380–8
- Jiang S *et al* 2009 Evaluation of breast tumor response to neoadjuvant chemotherapy with tomographic diffuse optical spectroscopy: case studies of tumor region-of-interest changes *Radiology* **252** 551–60
- Kim M N *et al* 2010 Noninvasive measurement of cerebral blood flow and blood oxygenation using near-infrared and diffuse correlation spectroscopies in critically brain-injured adults *Neurocrit Care* **12** 173–80

- Leff D R, Warren O J, Enfield L C, Gibson A, Athanasiou T, Patten D K, Hebden J, Yang G Z and Darzi A 2008 Diffuse optical imaging of the healthy and diseased breast: a systematic review *Breast Cancer Res. Treat.* **108** 9–22
- Lemieux P A and Durian D J 1999 Investigating non-gaussian scattering processes by using n th-order intensity correlation functions *J. Opt. Soc. Am. A* **16** 1651–64
- Mankoff D A, Dunnwald L K, Gralow J R, Ellis G K, Schubert E K, Tseng J, Lawton T J, Linden H M and Livingston R B 2003 Changes in blood flow and metabolism in locally advanced breast cancer treated with neoadjuvant chemotherapy *J. Nucl. Med.* **44** 1806–14
- Mastanduno M A *et al* 2014 Sensitivity of mri-guided near-infrared spectroscopy clinical breast exam data and its impact on diagnostic performance *Biomed. Opt. Express* **5** 3103–15
- McDermott G M *et al* 2007 Monitoring primary breast cancer throughout chemotherapy using fdg-pet *Breast Cancer Res. Treat.* **102** 75–84
- Meisamy S *et al* 2004 Neoadjuvant chemotherapy of locally advanced breast cancer: predicting response with *in vivo* (1)h mr spectroscopy—a pilot study at 4 t *Radiology* **233** 424–31
- Mesquita R C, Durduran T, Yu G, Buckley E M, Kim M N, Zhao C, Cho R, Sunar U and Yodh A G 2011 Direct measurement of tissue blood flow and metabolism with diffuse optics *Phil. Trans. R. Soc. A* **369** 4390–406
- O’Sullivan T D, Cerussi A E, Cuccia D J and Tromberg B J 2012 Diffuse optical imaging using spatially and temporally modulated light *J. Biomed. Opt.* **17** 071311
- Ramirez G *et al* 2016 Chemotherapeutic drug-specific alteration of microvascular blood flow in murine breast cancer as measured by diffuse correlation spectroscopy *Biomed. Opt. Express* **7** 3610–30
- Rastogi P *et al* 2008 Preoperative chemotherapy: updates of national surgical adjuvant breast and bowel project protocols b-18 and b-27 *J. Clin. Oncol.* **26** 778–85
- Roblyer D *et al* 2011 Optical imaging of breast cancer oxyhemoglobin flare correlates with neoadjuvant chemotherapy response one day after starting treatment *Proc. Natl Acad. Sci.* **108** 14626–31
- Sajjadi A Y *et al* 2017 Normalization of compression-induced hemodynamics in patients responding to neoadjuvant chemotherapy monitored by dynamic tomographic optical breast imaging (dtobi) *Biomed. Opt. Express* **8** 555–69
- Shang Y and Yu G 2014 A n th-order linear algorithm for extracting diffuse correlation spectroscopy blood flow indices in heterogeneous tissues *Appl. Phys. Lett.* **105** 133702
- Sledge G W, Mamounas E P, Hortobagyi G N, Burstein H J, Goodwin P J and Wolff A C 2014 Past, present, and future challenges in breast cancer treatment *J. Clin. Oncol.* **32** 1979–86
- Soliman H, Gunasekara A, Rycroft M, Zubovits J, Dent R, Spayne J, Yaffe M J and Czarnota G J 2010 Functional imaging using diffuse optical spectroscopy of neoadjuvant chemotherapy response in women with locally advanced breast cancer *Clin. Cancer Res.* **16** 2605–14
- Spinelli L, Torricelli A, Pifferi A, Taroni P, Danesini G and Cubeddu R 2005 Characterization of female breast lesions from multi-wavelength time-resolved optical mammography *Phys. Med. Biol.* **50** 2489–502
- Srinivasan S, Pogue B W, Brooksby B, Jiang S, Dehghani H, Kogel C, Wells W A, Poplack S P and Paulsen K D 2005 Near-infrared characterization of breast tumors *in vivo* using spectrally-constrained reconstruction *Technol. Cancer Res. Treat.* **4** 513–26
- Sunar U *et al* 2006 Noninvasive diffuse optical measurement of blood flow and blood oxygenation for monitoring radiation therapy in patients with head and neck tumors: a pilot study *J. Biomed. Opt.* **11** 064021
- Tromberg B J, Cerussi A, Shah N, Compton M, Durkin A, Hsiang D, Butler J and Mehta R 2005 Imaging in breast cancer: diffuse optics in breast cancer: detecting tumors in pre-menopausal women and monitoring neoadjuvant chemotherapy *Breast Cancer Res.* **7** 279–85
- Tromberg B J, Pogue B W, Paulsen K D, Yodh A G, Boas D A and Cerussi A E 2008 Assessing the future of diffuse optical imaging technologies for breast cancer management *Med. Phys.* **35** 2443–51
- Tromberg B J *et al* 2016 Predicting responses to neoadjuvant chemotherapy in breast cancer: acrin 6691 trial of diffuse optical spectroscopic imaging (dosi) *Cancer Res.* **76** 5933–44
- Ueda S *et al* 2012 Baseline tumor oxygen saturation correlates with a pathologic complete response in breast cancer patients undergoing neoadjuvant chemotherapy *Cancer Res.* **72** 4318–28
- Vinnicombe S J, MacVicar A D, Guy R L, Sloane J P, Powles T J, Knee G and Husband J E 1996 Primary breast cancer: mammographic changes after neoadjuvant chemotherapy, with pathologic correlation *Radiology* **198** 333–40

- Wang J, Jiang S, Li Z, diFlorio Alexander R M, Barth R J, Kaufman P A, Pogue B W and Paulsen K D 2010 *In vivo* quantitative imaging of normal and cancerous breast tissue using broadband diffuse optical tomography *Med. Phys.* **37** 3715–24
- Yazdi H S *et al* 2017 Mapping breast cancer blood flow index, composition, and metabolism in a human subject using combined dosi and dcs *J. Biomed. Opt.* **22** 045003
- Yeh E, Slanetz P, Kopans D B, Rafferty E, Georgian-Smith D, Moy L, Halpern E, Moore R, Kuter I and Taghian A 2005 Prospective comparison of mammography, sonography, and mri in patients undergoing neoadjuvant chemotherapy for palpable breast cancer *Am. J. Roentgenol* **184** 868–77
- Yu G 2012 Near-infrared diffuse correlation spectroscopy in cancer diagnosis and therapy monitoring *J. Biomed. Opt.* **17** 010901
- Zhou C *et al* 2007 Diffuse optical monitoring of blood flow and oxygenation in human breast cancer during early stages of neoadjuvant chemotherapy *J Biomed. Opt.* **12** 051903
- Zhu Q, Tannenbaum S, Hegde P, Kane M, Xu C and Kurtzman S H 2008 Noninvasive monitoring of breast cancer during neoadjuvant chemotherapy using optical tomography with ultrasound localization *Neoplasia* **10** 1028–40